Journal of Catalysis **186,** 134–146 (1999)
Article ID jcat.1999.2537, available online at http://www.idealibrary.com on IDEAL®

Catalytic Ramifications of Steam Deactivation of Y Zeolites: An Analysis Using 2-Methylhexane Cracking

G. Yaluris,*[,1] R. J. Madon,†[,2] and J. A. Dumesic*[,2]

*Center for Clean Industrial and Treatment Technologies, Department of Chemical Engineering, University of Wisconsin, Madison, Wisconsin 53706; and †Engelhard Corporation, 101 Wood Avenue, Iselin, New Jersey 08830

Received January 5, 1999; revised April 14, 1999; accepted April 15, 1999

Kinetic analysis of experimental data for 2-methylhexane cracking demonstrates that trends in activity and selectivity are well simulated by adjusting a single parameter that represents the acid strength of a Y-based FCC catalyst. This acid strength may be modified via steam deactivation, and we have experimentally corroborated acidity changes using ammonia microcalorimetry and infrared spectroscopy. Increased severity of steam treatment reduces the number and strength of catalyst acid sites, and it leads to a reduction in the turnover frequency of all surface processes and a decrease in overall site time yield. Steaming of the catalyst does not change the fundamental chemistry involved in catalytic cracking. However, change in acidity caused by steaming alters product selectivity by changing relative rates of various catalytic cycles in the cracking process. For example, steam treatment increases olefin selectivity by favoring catalytic cycles that produce olefins. © 1999 Academic Press

INTRODUCTION

Over the past several years, we have used kinetic analyses of experimental data for isobutane and 2-methylhexane cracking (1–4) to gain insights into cracking processes. We have obtained turnover frequencies (TOF) of individual steps in reaction schemes and estimated relative surface coverages by reaction intermediates. We have suggested the importance of the enthalpy of stabilization of surface carbenium ions relative to that of a surface proton. By analyzing various catalytic cycles (2–5), we have described the roles that different reactions play in determining overall rate and product selectivities during catalytic cracking. In these investigations, we have altered catalyst properties via steam treatment.

Steam, as is well known, dealuminates the framework of a Y zeolite (6, 7) as well as destroys some of the zeolite. It is used to mimic deactivation effects in a commercial cracking process. Various studies have been carried out to understand the ramifications of steam treatment on USY catalysts and the effects of resulting nonframework or extraframework (EFAl) aluminum species. As examples, we note that Lunsford *et al.* (8) and Beyerlein *et al.* (9) indicate an interaction between EFAl and Brønsted acid sites leading to increased strength of the latter, while Kung *et al.* (10) indicate that mild steaming increases accessibility to active sites thus enhancing cracking activity. Others have proposed (11, 12) that EFAl may lead to site blocking or crowding effects leading to decreased activity. The extent to which steaming plays a consequential role in catalytic cracking as well as some inconsistencies in the literature may ensue from differences in the severity of steam treatment and the nature of the starting and steamed catalyst. Wang *et al.* (13), for example, note that the effect on catalyst reactivity depends on whether, after steaming, framework Al (Al_F) content is greater than 15 Al_F/unit cell.

In commercial fluid catalytic cracking (FCC), aged catalysts give different product yields than fresh catalysts. Some of our work has been an effort to understand this observation. Pine *et al.* (14) argued that hydride ion transfer, a key bimolecular reaction in catalytic cracking, requires next nearest Al_F sites, and therefore catalysts with high unit cell sizes, i.e., catalysts with low Si/Al_F ratios, are more active for such reactions. This explanation was later refuted (15–17). Corma and co-workers (15, 16) concluded that catalytic and adsorptive changes after dealumination were caused by increased hydrophobicity of the increasingly siliceous zeolite, whereas Madon (17) proposed that hydride ion transfer was dependent on the location and strength of Brønsted acid sites.

Our work (2, 4, 18) has consistently shown that severe steaming not only reduces the number of Brønsted acid sites on USY-based FCC catalysts but also appears to decrease acid strength. In this paper, we use a wide range of steaming severities to vary catalytic properties and thus present a more detailed description of how steaming influences the kinetics of catalytic cracking. Using the same modeling parameters as in Ref. (4), we have probed the fundamental changes caused by steam dealumination in the catalytic

[1] Current address: Grace Davison, 7500 Grace Dr., Columbia, MD 21044.

[2] To whom correspondence should be addressed.

0021-9517/99 $30.00

reactions of 2-methylhexane cracking. This paper also briefly explores kinetic implications of alkoxy versus carbenium ion surface intermediates and reinforces the importance of the relative enthalpy of formation of reactive carbenium ions.

EXPERIMENTAL

We carried out our experimental study on six USY-based FCC catalysts that were all prepared from a single starting catalyst made via the Engelhard *in situ* zeolite crystallization process (19–21). This starting catalyst, after exchange with ammonium nitrate to remove sodium cations, contained 0.3 wt% Na_2O and had no rare earth cations. We steamed this catalyst by fluidizing it in 100% steam under six different conditions to obtain the samples for our study. Table 1 lists steaming conditions and properties of these catalysts. The microporous surface area of each sample, which is assumed to be largely that of the zeolite component, was calculated from the nitrogen BET surface area of the entire sample minus the surface area of pores larger than 2 nm in diameter, obtained as a *t* plot. X-ray diffraction measurements, using a Si standard, gave unit cell sizes (ucs), from which we determined the framework aluminum per unit cell by using the correlation given by Sohn *et al.* (22) for Y zeolites.

We performed diffuse-reflectance infrared spectroscopy of adsorbed pyridine in a Spectra Tech controlled-environment chamber in a Perkin–Elmer 1750 spectrometer to measure the number of Brønsted and Lewis acid sites. We used extinction coefficients specifically obtained for this instrument by using calibrated alumino-silicate samples. Details of these experiments are given elsewhere (18). We used the number of Brønsted acid sites measured via this approach in our microkinetic analyses.

To further probe the acid site strength distributions of these catalysts, we measured differential heats of ammonia adsorption at 423 K using the microcalorimetric apparatus and procedure described in Refs. (2, 18, 23). Before ammonia was adsorbed on the catalysts, they were calcined at 723 K for 2 h in static oxygen that was periodically evacuated and replenished, followed by a final evacuation for 1.5 h at the same temperature.

We carried out kinetic experiments in a fixed-bed flow unit using Pyrex reactors, as described earlier (1, 3, 4). The top of the reactor, filled with quartz rings, served as a preheating zone, while the catalyst was supported in the lower third of the reactor with quartz wool. We adjusted catalyst amounts and 2-methylhexane flow rates to obtain about 15% conversion over all catalysts. For more severely steamed catalysts (USY-4, USY-5, and USY-6 in Table 1) we conducted kinetic studies using a larger reactor because of the larger amount of catalyst needed to obtain the desired conversion. The size of the reactor influences the amount of products from gas phase thermal reactions and, thus, it affects the correction necessary to determine the products from catalytic cracking (4, 24). We used a mixture of 10 mol% 2-methylhexane in He (Liquid Carbonic, 99.999% purity) in all experiments and collected reaction products in 20-cm^3 sampling loops of a multiport Valco valve. We collected the first sample after ~1 min of reaction time, and typically four samples were collected at time intervals of 1–2 min. The data reported here are usually from the first loop. We did not observe any selectivity changes from one loop to the other, while conversions changed only slightly with time on stream. We purged the catalyst between runs with flowing He (200 cm^3/min) for about 2 h, and then regenerated it in flowing air (200 cm^3/min) at 773 K for 8 h.

We note that by using a small gasoline-range alkane, 2-methylhexane, we are able to study the catalytic role of Y

TABLE 1

Properties of Catalysts USY-1, USY-2, USY-3, USY-4, USY-5, and USY-6

	Catalyst					
	USY-1	USY-2	USY-3	USY-4	USY-5	USY-6
Steaming temperature (K)	840	975	1030	1060	1060	1090
Steaming time (h)	2	2	2	2	5	3
Zeolite surface area (m^2/g)	268	247	233	205	203	185
Total surface area (m^2/g)	417	391	371	335	332	311
Zeolite content[a] (%)	37	34	32	29	28	26
Unit cell size (Å)	24.40	24.37	24.33	24.28	24.27	24.26
Al_F[b]/unit cell	17.35	14.14	9.85	4.50	3.43	2.36
Al_F (μmol)/g of catalyst	554	415	272	113	83	53
Si/Al_F	10.1	12.6	18.5	42	55.0	80
Brønsted sites (μmol/g)	360	157	129	30	18	18
Lewis sites (μmol/g)	311	205	166	50	36	40
Ratio of Brønsted to Lewis acid sites	1.16	0.77	0.78	0.6	0.5	0.45

[a] From BET measurements assuming that the surface area of pores <2 nm is mainly due to the Y zeolite.
[b] Number of framework Al atoms.

zeolite in these commercial FCC catalysts, since the nonzeolitic portion of such catalysts is relatively inactive for cracking of small paraffinic hydrocarbons.

MODEL DEVELOPMENT

As we have shown elsewhere, a kinetic model may be used to quantitatively analyze catalytic cycles that are operative during catalytic cracking of model hydrocarbons over FCC catalysts (2–5). This model provides information about changes in the relative rates of various cycles with reaction conditions and shows how these changes affect observed catalytic activity and selectivity. Importantly, since this model incorporates catalyst properties like the number of Brønsted acid sites and acid strength, it helps us to quantify and better understand how changes in catalyst properties affect catalytic behavior. Here, we use the model previously developed (4) for 2-methylhexane cracking to analyze and relate the effects of steam treatment on the activity and selectivity for catalytic cracking.

We have presented elsewhere details of the development of our kinetic model for cracking 2-methylhexane on Y-zeolite-based catalysts (3, 4, 24). In short, the model consists of two components: a reaction scheme that describes the cracking of 2-methylhexane and accounts for all important reaction products and a thermodynamically consistent set of preexponential factors and activation energies. The reaction scheme, shown in Fig. 1, is based on carbocation chemistry and includes carbenium ion initiation, oligomerization/β-scission, isomerization, hydride ion transfer, and olefin adsorption–desorption reactions. While our reaction scheme does not explicitly include gas phase radical cracking, we account for such cracking taking place in the preheat section of the reactor by conducting kinetic experiments in an empty reactor at the same temperature and flow rate used in the catalytic experiments. In the model, we include reaction products obtained from these experiments as part of the feed to the catalyst bed.

We estimated preexponential factors using transition state theory,

$$A = \frac{k_B T}{h} e^{\frac{\Delta S^{o\ddagger}}{R}}, \qquad [1]$$

where k_B and h are the Boltzmann and Planck constants, respectively, and $\Delta S^{o\ddagger}$ is the standard entropy change from reactants to the transition state. We have previously described the procedure to obtain thermodynamically consistent estimates of entropies of all species included in the reaction scheme of Fig. 1 (1, 3, 24).

We obtained a thermodynamically consistent set of activation energies using the Evans–Polanyi correlation (1, 25)

$$E_a = E_o + 0.5\Delta H, \qquad [2]$$

where ΔH is the heat of reaction and E_o is a constant for a given reaction family defined as a set of reactions with similar reaction chemistry (3, 4). We calculated or estimated the heats of reaction for the steps in Fig. 1 from gas phase thermodynamic data available in the literature (1) and given in Table 2. We obtained enthalpies of formation of surface species from gas phase data adjusted for surface adsorption by using a single parameter, ΔH_+. The latter represents the heat of stabilization of a carbenium ion complex relative to the heat of stabilization of a proton on the acid

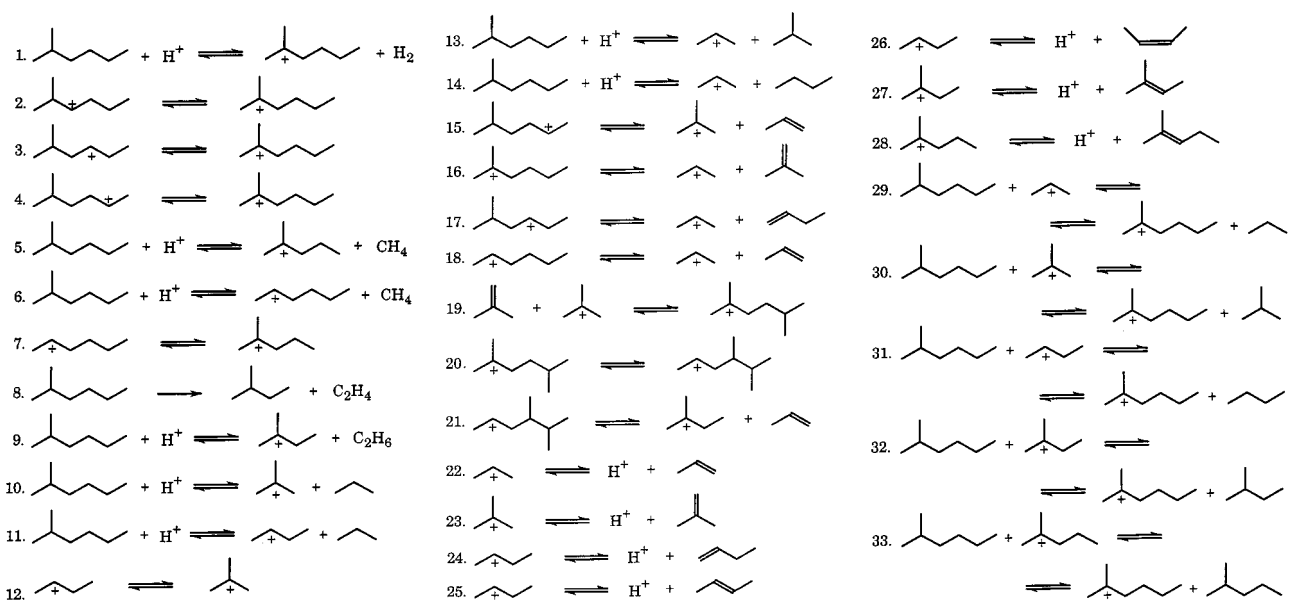

FIG. 1. Reaction scheme for 2-methylhexane cracking.

TABLE 2

Reaction Enthalpy Changes and Activation Energies (kcal/mol) for Catalysts USY-1 through USY-6 Estimated at 773 K for Reaction Steps in 2-Methylhexane Cracking

		USY-1 $E_o(8)=23.3$ $\Delta H_+=165.4$		USY-2 $E_o(8)=23.4$ $\Delta H_+=166.1$		USY-3 $E_o(8)=24.9$ $\Delta H_+=167.7$		USY-4 $E_o(8)=24.9$ $\Delta H_+=169.0$		USY-5 $E_o(8)=25.9$ $\Delta H_+=169.8$		USY-6 $E_o(8)=27.1$ $\Delta H_+=171.6$	
	E_o	$E_{a,for}$	$E_{a,rev}$	$E_{a,for}$	$E_{a,rev}$	$E_{a,for}$	$E_{a,rev}$	$E_{a,for}$	$E_{a,rev}$	$E_{a,for}$	$E_{a,rev}$	$E_{a,for}$	$E_{a,rev}$
Step 1	37.4	32.9	41.8	33.3	41.4	34.1	40.6	34.8	39.9	35.2	39.6	36.1	38.6
Step 2	0	0	18.2	0	18.2	0	18.2	0	18.2	0	18.2	0	18.2
Step 3	0	0	18.2	0	18.2	0	18.2	0	18.2	0	18.2	0	18.2
Step 4	0	0	18.2	0	18.2	0	18.2	0	18.2	0	18.2	0	18.2
Step 5	46.3	34.3	58.4	34.6	58.0	35.4	57.2	36.1	56.5	36.5	56.1	37.4	55.2
Step 6	39.7	37.7	41.8	38.1	41.4	38.9	40.6	39.5	39.9	39.9	39.5	40.8	38.6
Step 7	0	0	20.0	0	20.0	0	20.0	0	20.0	0	20.0	0	20.0
Step 8	*	34.1	12.5	34.2	12.6	35.7	14.1	35.7	14.2	36.7	15.1	37.8	16.3
Step 9	46.3	35.8	56.8	36.2	56.5	37.0	55.7	37.6	55.0	38.0	54.6	38.9	53.7
Step 10	70.0	60.5	79.5	60.9	79.1	61.7	78.3	62.3	77.6	62.7	77.2	63.6	76.3
Step 11	31.7	31.0	32.3	31.4	32.0	32.2	31.2	32.8	30.5	33.2	30.1	34.1	29.2
Step 12	0	0	17.6	0	17.6	0	17.6	0	17.6	0	17.6	0	17.6
Step 13	31.7	31.0	32.3	31.4	31.9	32.2	31.1	32.8	30.5	33.2	30.1	34.1	29.2
Step 14	39.7	40.0	39.5	40.4	39.1	41.2	38.3	41.9	37.6	42.3	37.2	43.2	36.3
Step 15	35.1	36.3	33.8	36.3	33.8	36.3	33.8	36.3	33.8	36.3	33.8	36.3	33.8
Step 16	29.8	48.2	11.4	48.2	11.4	48.2	11.4	48.2	11.4	48.2	11.4	48.2	11.4
Step 17	20.0	31.2	8.8	31.2	8.8	31.2	8.8	31.2	8.8	31.2	8.8	31.2	8.8
Step 18	29.8	40.4	19.3	40.4	19.3	40.4	19.3	40.4	19.3	40.4	19.3	40.4	19.3
Step 19	35.1	25.4	44.7	25.4	44.7	25.4	44.7	25.4	44.7	25.4	44.7	25.4	44.7
Step 20	0	18.0	0	18.0	0	18.0	0	18.0	0	18.0	0	18.0	0
Step 21	18.7	20.4	17.1	20.4	17.1	20.4	17.1	20.4	17.1	20.4	17.1	20.4	17.1
Step 22	0	19.8	0	19.0	0	17.4	0	16.1	0	15.3	0	13.5	0
Step 23	0	35.8	0	35.1	0	33.5	0	32.2	0	31.4	0	29.6	0
Step 24	0	22.1	0	21.3	0	19.7	0	18.4	0	17.7	0	15.8	0
Step 25	0	19.4	0	18.6	0	17.0	0	15.7	0	14.9	0	13.1	0
Step 26	0	19.8	0	19.0	0	17.4	0	16.1	0	15.3	0	13.5	0
Step 27	0	35.7	0	35.0	0	33.3	0	32.1	0	31.3	0	29.5	0
Step 28	0	37.5	0	36.7	0	35.1	0	33.8	0	33.0	0	31.2	0
Step 29	22.5	12.6	32.5	12.6	32.5	12.6	32.5	12.6	32.5	12.6	32.5	12.6	32.5
Step 30	25.2	24.1	26.3	24.1	26.3	24.1	26.3	24.1	26.3	24.1	26.3	24.1	26.3
Step 31	20.4	11.4	29.4	11.4	29.4	11.4	29.4	11.4	29.4	11.4	29.4	11.4	29.4
Step 32	26.2	26.0	26.4	26.0	26.4	26.0	26.4	26.0	26.4	26.0	26.4	26.0	26.4
Step 33	22.5	22.9	22.2	22.9	22.2	22.9	22.2	22.9	22.2	22.9	22.2	22.9	22.2

site. This parameter is also equal to the heat of formation of a surface carbenium ion by reaction of a gaseous olefin with a Brønsted acid site relative to the heat of formation of a gaseous carbenium ion by reaction of an olefin with a gaseous proton.

In general, a gaseous proton interacts ($\Delta H_{Z\text{-}H}+$) more strongly with a negative zeolite surface (Z^-) than a gaseous carbenium ion interacts ($\Delta H_{Z\text{-}AH}+$) with the surface. Therefore, the heat of formation of a gaseous carbenium ion, ΔH_{gas}, by reaction of an olefin with a gaseous proton is more negative than the heat of formation of a surface carbenium ion, $\Delta H_{\text{surface}}$, by reaction of a gaseous olefin with a Brønsted acid site. We define $Q_i = -\Delta H_i$, such that $Q_{Z\text{-}H}+$, $Q_{Z\text{-}AH}+$, Q_{gas}, and Q_{surface} are positive quantities. By constructing the thermodynamic cycle in Fig. 2, we note that

$$0 = Q_{Z\text{-}H+} - Q_{\text{gas}} - Q_{Z\text{-}AH+} + Q_{\text{surface}}, \qquad [3]$$

from which we write,

$$Q_{Z\text{-}H+} - Q_{Z\text{-}AH+} = Q_{\text{gas}} - Q_{\text{surface}}. \qquad [4]$$

We then define ΔH_+ as

$$\Delta H_+ = Q_{Z\text{-}H+} - Q_{Z\text{-}AH+} = Q_{\text{gas}} - Q_{\text{surface}}. \qquad [5]$$

The adjustable parameter, ΔH_+, represents the only parameter in our model that reflects a surface property and it is an important component of our analyses. We discuss this parameter in more detail in later sections. The other adjustable parameters are the Evans–Polanyi constants. We assumed the number of active sites to be equal to the measured number of Brønsted acid sites (Table 1).

The data available here on each catalyst are limited to a single conversion of ~15%. Therefore, to obtain meaningful results from the optimization process, we have limited

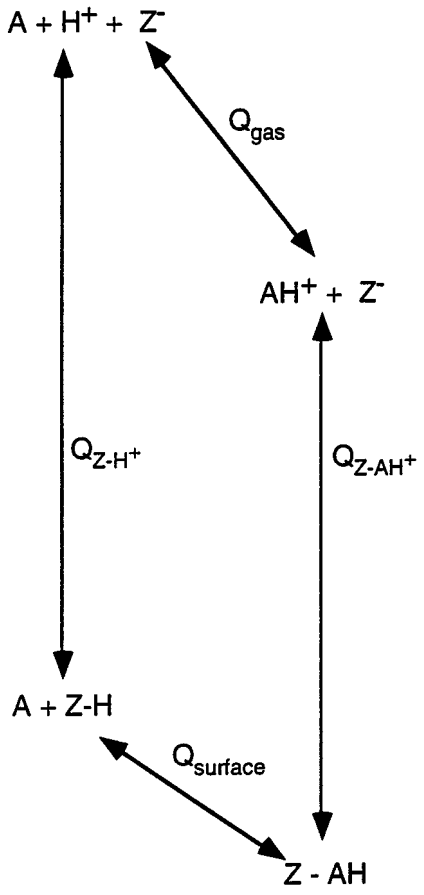

FIG. 2. Schematic representation for interactions between an olefin (A) and a Brønsted acid site (Z-H).

the number of adjustable parameters. Our goal here was not to simulate the experimental data in detail, but to obtain estimates and trends for ΔH_+ with varying steaming severity and to ascertain the relationship between ΔH_+ and the kinetic results. The catalysts studied here are similar to those used to develop the microkinetic model (4). Therefore, we estimated the kinetic parameters for each catalyst using Evans–Polanyi parameters obtained during our earlier analyses of 2-methylhexane cracking over a catalyst with steaming conditions intermediate to the range of steaming conditions used here. We used the parameters of catalyst USY-S1 in Ref. (4) steamed for 2 h at 1030 K. While fitting the kinetic data for catalysts USY-1 through USY-6, we allowed the value of ΔH_+ to change, since this parameter is the only one associated with the catalyst surface that changes with steaming. Since step 8, Fig. 1, for ethylene formation is not considered an elementary step, changes in the rate of this step with steaming may not follow changes represented by ΔH_+; therefore, we allowed the Evans–Polanyi parameter of this step to change with steaming. In Table 2 we give the estimated values of these parameters and the activation energies of the reaction steps in Fig. 1 for catalysts USY-1 through USY-6.

As noted above, ΔH_+ is the single parameter in the model that represents the acidity of the catalyst. We chose the definition of ΔH_+ in this work to be consistent with our previous work, i.e., the heat of stabilization of a carbenium ion *reactive intermediate* relative to the heat of stabilization of a proton on the acid site. Although carbenium ion intermediates have been observed on solid acid surfaces (26), recent experimental (27) and theoretical studies (28) have shown that adsorbed intermediates on alumino-silicate acid catalysts are similar to neutral alkoxy species, while transition states for reactions involving these alkoxy species are similar to positively charged carbenium ions. Therefore, we consider here whether the parameter ΔH_+ should be defined more correctly as the heat of stabilization of a carbenium ion transition state relative to the heat of stabilization of a proton on the acid site. The following example demonstrates the kinetic equivalence of these two definitions for ΔH_+.

Consider a three-step sequence for the overall isomerization of olefin A to isomer B over acid sites Z-H:

Sequence I

1. $A + Z\text{-}H \rightleftharpoons Z\text{-}AH$
2. $Z\text{-}AH \rightleftharpoons Z\text{-}BH$
3. $Z\text{-}BH \rightleftharpoons B + Z\text{-}H.$

If the first step is quasi-equilibrated, then the forward rate, r_{for}, of the acid catalyzed reaction is

$$r_{\text{for}} = \frac{k_B T}{h} c^{\ddagger}, \qquad [6]$$

where $c^{\ddagger}$ is the transition state concentration. Since the transition state by definition is in equilibrium with Z-AH and species A,

$$r_{\text{for}} = \frac{k_B T}{h} K^{\ddagger} K_{\text{eq1}} P_A \theta_{ZH}, \qquad [7]$$

where $K^{\ddagger}$ is the equilibrium constant between Z-AH and the transition state, K_{eq1} is the equilibrium constant for step 1, P_A is the pressure of species A, and θ_{ZH} is the fraction of available acid sites. At our experimental conditions, surface coverage by adsorbed species is small, and θ_{ZH} is therefore approximately equal to 1. Depending on the definition of ΔH_+, the latter is embedded in either K_{eq1} or $K^{\ddagger}$ of Eq. [7]. We note, however, that the product of $K^{\ddagger}$ and K_{eq1} is equal to the equilibrium constant for the formation of the activated complex from Z-H and species A; therefore, this overall equilibrium constant is dependent only on the nature of the activated complex, i.e., it is independent of the nature of intermediate species Z-AH.

If ΔH_+ is defined as the heat of stabilization of a carbenium ion reactive intermediate relative to the heat of stabilization of a proton on the acid site, then the value of $K^{\ddagger}$ is independent of ΔH_+ (since we have assumed that Z-AH

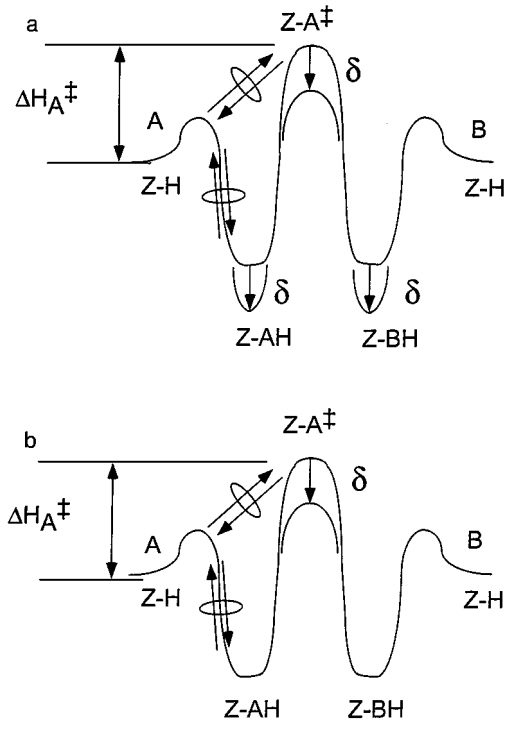

FIG. 3. Schematic representations of olefin isomerization on a strong and weak acid when (a) the carbenium ion is a surface intermediate and (b) the carbenium ion is a transition state.

and *Z-BH* are both carbenium ions). The heat of adsorption for step 1 is equal to $-Q_{\text{gas}} + \Delta H_+$, and K_{eq1} is given by

$$K_{\text{eq1}} = e^{\frac{\Delta S^{\text{o}}_{\text{ads}}}{R}} e^{\frac{-(-Q_{\text{gas}}+\Delta H_+)}{RT}}, \qquad [8]$$

where $\Delta S^{\text{o}}_{\text{ads}}$ is the standard entropy change of adsorption. The rate of the acid catalyzed reaction is thus proportional to $e^{-\Delta H_+/RT}$. This situation is represented schematically in Fig. 3a. Here we compare catalysts having different acid strengths. As the acid strength increases, species *Z-AH* and *Z-BH* and the activated complex $Z\text{-}A^{\ddagger}$ are all stabilized by δ. Since step 1 is quasi-equilibrated, the apparent activation enthalpy for the overall rate is $\Delta H^{\ddagger}_A$, and this value is also stabilized by δ.

If ΔH_+ is defined as the heat of stabilization of a carbenium ion *transition state* relative to the heat of stabilization of a proton on the acid site, then the value of K_{eq1} is independent of ΔH_+, since the adsorbed species are neutral alkoxy species. $K^{\ddagger}$ is given by

$$K^{\ddagger} = e^{\frac{\Delta S^{\text{o}\ddagger}}{R}} e^{\frac{-\Delta H^{\text{o}\ddagger}}{RT}}, \qquad [9]$$

where $\Delta S^{\text{o}\ddagger}$ and $H^{\text{o}\ddagger}$ are the standard entropy and enthalpy changes of activation for step 2. To determine the activation enthalpy $\Delta H^{\text{o}\ddagger}_2$ for step 2 in terms of ΔH_+, we express this step as a series of the following four processes:

Sequence II (for step 2 in Sequence I)

2a. $Z\text{-}AH \rightarrow A_{(\text{gas})} + Z\text{-}H$

2b. $Z\text{-}H \rightarrow H^+_{(\text{gas})} + Z^-$

2c. $A_{(\text{gas})} + H^+_{(\text{gas})} \rightarrow (AH^+)^{\ddagger}_{(\text{gas})}$

2d. $(AH^+)^{\ddagger}_{(\text{gas})} + Z^- \rightarrow Z\text{-}AH^{\ddagger}$

This reaction sequence is similar to the steps shown in Fig. 2, with the gas phase carbenium ion, AH^+ being replaced by the gas phase carbenium ion transition state, $(AH^+)^{\ddagger}$. The heats of these steps are equal to (2a) the heat of desorption of species *A* from the catalyst, a positive value equal to Q_{surface}; (2b) the heat for removal of a proton from the catalyst, a positive value equal to $Q_{\text{Z-H+}}$; (2c) the heat for reaction of gaseous species *A* with a proton to make the gaseous carbenium ion transition state, a negative value equal to $-Q_{\text{gas}\ddagger}$; and (2d) the heat of interaction of the gaseous transition state with the catalyst, a negative value equal to $-Q_{\text{Z-(AH}^+)\ddagger}$. Therefore, the enthalpy of activation of step 2 is given by

$$\begin{aligned}\Delta H^{\text{o}\ddagger}_2 &= Q_{\text{surface}} + Q_{Z\text{-}H^+} - Q_{\text{gas}\ddagger} - Q_{Z\text{-}(AH^+)\ddagger} \\ &= (Q_{\text{surface}} - Q_{\text{gas}\ddagger}) + (Q_{Z\text{-}H} - Q_{Z\text{-}(AH^+)\ddagger}) \\ &= E^{\text{o}}_{\text{a}} + \Delta H_+, \end{aligned} \qquad [10]$$

where E^{o}_{a} is the activation energy when ΔH_+ is equal to zero (i.e., $E^{\text{o}}_{\text{a}} = Q_{\text{surface}} - Q_{\text{gas}\ddagger}$). We note in this case that Q_{surface} does not depend on ΔH_+, since *Z-AH* is a neutral alkoxy species. Also we note that this definition for ΔH_+ is the heat of stabilization of a carbenium ion transition state relative to the heat of stabilization of a proton on the acid site. From Eqs. [7], [9], and [10], we see that the acid catalyzed reaction is again proportional to $e^{-\Delta H_+/RT}$. This situation is represented schematically in Fig. 3b. As acid strength increases, the activated complex $Z\text{-}A^{\ddagger}$ is stabilized by δ and species *Z-AH* and *Z-BH* remain unchanged. Again, since step 1 is quasi-equilibrated, the apparent activation enthalpy for the overall rate is $\Delta H^{\ddagger}_A$, and this value is stabilized by δ.

In summary, the two different definitions for ΔH_+ lead to equivalent relations for the effect of this parameter on the rate of an acid catalyzed reaction; i.e., the rate is proportional to $e^{-\Delta H_+/RT}$ in both cases. This equivalence is also demonstrated schematically in Figs. 3a and 3b; i.e., the apparent activation energy, $\Delta H^{\ddagger}_A$, is the same in both cases and is shifted by δ.

The cases discussed above are two extremes in which adsorbed species are either carbenium ions or neutral alkoxy intermediates. Various workers (e.g., 28, 29) recently showed that an adsorbed intermediate on the acid surface has a partial positive charge that transmutes during reaction to a more positively charged activated complex. In such a

case the enthalpy change ΔH_+ would be embedded in both K_{eq1} and $K^{\ddagger}$ of Eq. [7]. Again, this situation would lead to the same changes as shown in Figs. 3a and 3b with the apparent activation energy showing the same behavior as in the two extreme cases.

RESULTS

Catalysts

Table 1 shows changes in catalyst properties with severity of steam treatment. As this severity increases from USY-1 to USY-6, zeolite content and unit cell size decrease. As noted by Chen *et al.* (18), steaming affects framework Al content to a larger extent than zeolite surface area. Dealumination of the framework results in a large decrease in the number of Brønsted acid sites; and although Lewis acid sites also decrease, the ratio of Brønsted to Lewis acid sites decreases monotonically with increased steaming. In agreement with others (18, 30–32), we observe that the number of Brønsted acid sites expressed as micromoles per gram of catalyst does not change linearly with the number of framework aluminum species expressed either per unit cell or per gram of catalyst (Fig. 4). This behavior may be caused by cations other than protons in the zeolite (e.g., Na^+, nonframework Al) balancing the excess charge or caused by the inaccessibility of Al sites in sodalite cages. Since sites in sodalite cages are considered to be weak acid sites, they may interact weakly with pyridine which desorbs from these sites at the temperature used to determine the number of Brønsted acid sites.

Figure 5 shows differential heats of ammonia adsorption at 423 K versus adsorbate coverage on catalysts USY-1, USY-3, and USY-6. Figure 6 shows histograms of acid site strength distributions for these catalysts. We obtained these

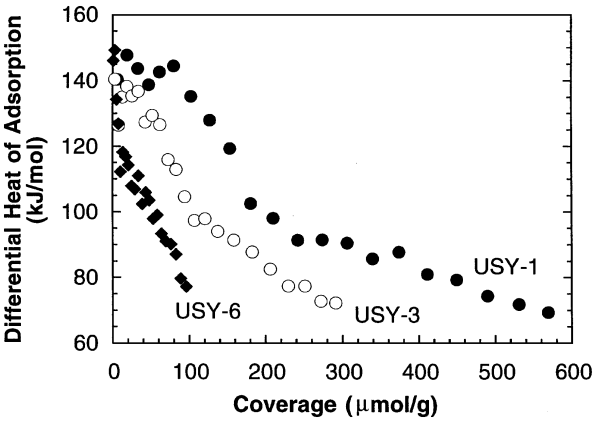

FIG. 5. Differential heats of ammonia adsorption on USY-1, USY-3, and USY-6 at 423 K.

histograms by fitting differential heats of adsorption with a polynomial and then using it to estimate the amount of adsorbed ammonia within a range of differential heats. In agreement with earlier results (2, 4, 18), steaming the catalysts not only decreases the number of acid sites, but also decreases the average acid strength of these sites. About 20% of acid sites on catalyst USY-1 adsorb ammonia with heats around 140 kJ/mol. Increasing steaming severity from 840 to 1030 K reduces the percentage of acid sites on USY-3 that adsorb ammonia at 140 kJ/mol by more than 40%, and it increases the relative number of sites

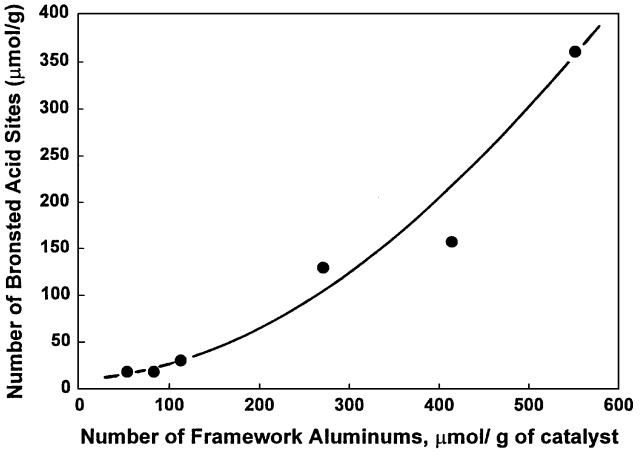

FIG. 4. Nonlinear relationship of framework Brønsted acid sites for catalysts USY-1 through USY-6 with a decrease in framework Al atoms per gram of catalyst.

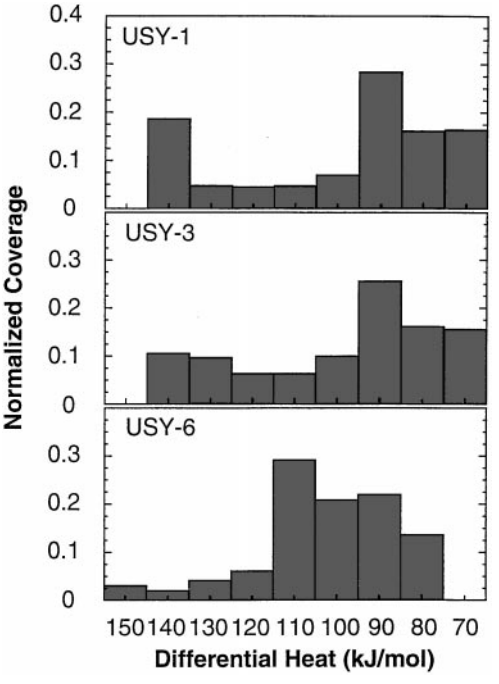

FIG. 6. Acid site strength distributions from NH_3 microcalorimetry at 423 K for catalysts USY-1, USY-3, and USY-6. Coverage normalized with respect to the total number of acid sites for each catalyst.

TABLE 3

Experimental Data and Model Predictions for 2-Methylhexane Cracking over Catalysts USY-1 through USY-6 at 773 K

	Catalyst											
	USY-1		USY-2		USY-3		USY-4		USY-5		USY-6	
S_V^{-1}(g/h/mol)	1.2		4.1		10.5		62.5		102		185	
Pressure (kPa)	125.2		124.6		122.2		136.2		142.1		141.4	
Conversion(%)	15.0		13.9		15.9		15.8		14.5		13.6	
	Exp	Model	Exp	Model	Exp	Model	Exp	Model	Exp	Model	Exp	Model
Hydrogen	0.155	0.073	0.115	0.074	0.167	0.091	0.160	0.101	0.303	0.088	0.282	0.095
Methane	0.064	0.055	0.054	0.057	0.077	0.075	0.106	0.080	0.105	0.075	0.094	0.087
Ethylene	0.036	0.052	0.043	0.059	0.044	0.060	0.096	0.078	0.046	0.061	0.047	0.066
Ethane	0.014	0.014	0.010	0.014	0.013	0.018	0.027	0.020	0.018	0.018	0.021	0.020
Propylene	1.125	1.120	0.976	0.933	1.164	0.940	1.212	0.903	1.163	0.660	1.095	0.553
Propane	0.306	0.324	0.264	0.287	0.257	0.322	0.236	0.343	0.131	0.274	0.126	0.267
Isobutane	0.869	0.861	0.727	0.706	0.796	0.693	0.756	0.656	0.655	0.469	0.589	0.376
n-Butane	0.125	0.135	0.105	0.103	0.109	0.09	0.112	0.076	0.071	0.047	0.061	0.027
C_4 olefins	0.422	0.415	0.356	0.381	0.439	0.446	0.491	0.480	0.509	0.399	0.51	0.405
2-Methyl-2-butene	0.008	0.01	0.008	0.001	0.008	0.013	0.009	0.014	0.007	0.011	0.009	0.011
Isopentane	0.052	0.036	0.055	0.039	0.051	0.031	0.044	0.049	0.038	0.028	0.033	0.024
Isohexane	0.028	0.019	0.027	0.018	0.033	0.021	0.024	0.024	0.045	0.021	0.033	0.019

Note. All values are mole percentages of the reactor effluent system.

that adsorb ammonia with lower differential heats between 105 and 135 kJ/mol. When we increase steaming severity further to 3 h at 1090 K, a few strong acid sites still appear that adsorb ammonia with differential heats around 150 kJ/mol. These strong sites, ca. 140 to 150 kJ/mol, are Lewis acid centers as discussed in detail by Chen *et al.* (18). However, most of the acid sites that remain on USY-6 are weaker than those on USY-1 and USY-3. More than 70% of the acid sites on USY-6 adsorb ammonia with differential heats between 85 and 115 kJ/mol. For comparison, only 40% of the acid sites of USY-1 and 43% of the acid sites of USY-3 have such low differential heats of ammonia adsorption.

Kinetic Analyses

In Table 3, we present experimental data and model predictions. Figure 7 shows changes in ΔH_+ with unit cell sizes. Note that unit cell size by itself is not an important property; it is used here as a fingerprint to reflect the extent of steaming severity. Figure 8 compares experimental and predicted site time yields (STY), molecules of 2-methylhexane converted per Brønsted acid site per second, versus ΔH_+ for all catalysts studied. Figures 9a and 9b compare experimental and predicted site time yields of paraffins and olefins produced with three or more carbon numbers versus ΔH_+. These data demonstrate that, despite the limited number

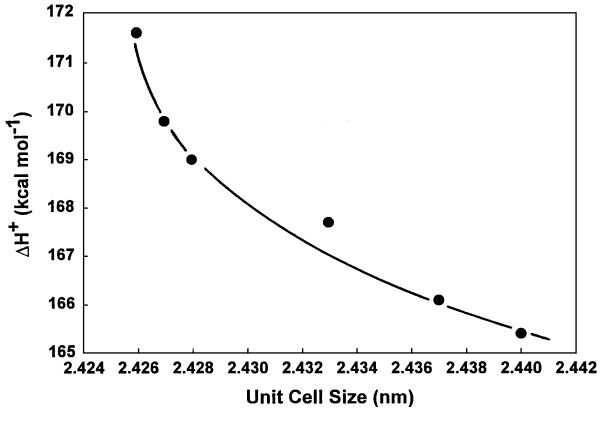

FIG. 7. Model prediction of ΔH_+ for catalysts USY-1 through USY-6 versus steaming severity as represented by unit cell sizes.

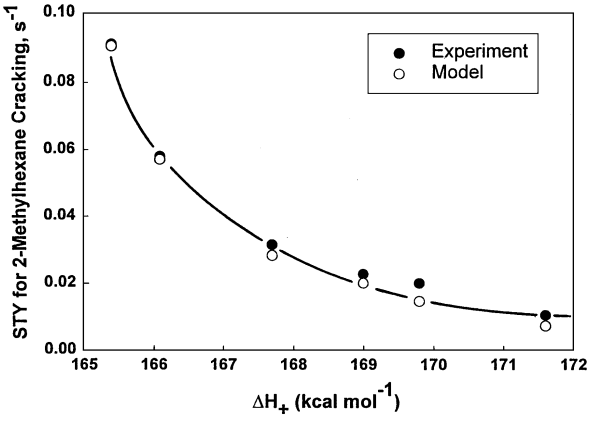

FIG. 8. Simulated and experimental site time yields (molecules converted per site per second) for 2-methylhexane conversion over USY-1 through USY-6 at 773 K and 15% conversion versus ΔH_+.

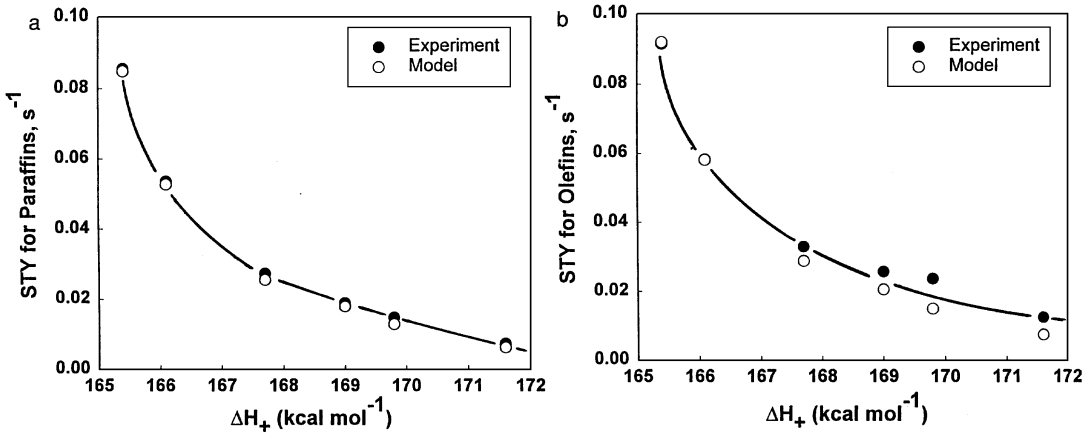

FIG. 9. Simulated and experimental site time yields for (a) paraffin and (b) olefin formation at 773 K and 15% 2-methylhexane conversion versus ΔH_+.

of adjustable parameters, our model accurately describes the essential trends of experimental data with steaming severity of USY-based FCC catalysts. Steaming results in lower values of STY and lower rates of paraffin and olefin formation, although olefin selectivity increases. From catalyst USY-1 to USY-6, while activity decreases by a factor of 9, the olefin to paraffin ratio increases from 1.12 to 1.92.

Table 3 and Figs. 9a and 9b show that, although experimental trends with steaming are described for all species, discrepancies between model predictions and experimentally observed values of individual species increase with severity of steam treatment. Model simulation of olefin formation is accurate for mildly steamed catalysts, but for severely steamed samples olefin production is underestimated resulting in paraffin to olefin ratios being overestimated. Propane is generally overpredicted, while C_4, C_5, and C_6 paraffins are under predicted. The model also underpredicts propylene formation, while it overpredicts the formation of C_5 and C_6 olefins. Some of these discrepancies are caused by uncertainties in parameter estimation. Kinetic parameters of our model are necessary approximations of actual values. Ordinarily, we have allowed (1, 4) the Evans–Polanyi parameters of initiation steps to change during optimization to compensate for changes in catalyst acid strength caused by steaming. But here, since we do not allow any parameters, other than ΔH_+ and the Evans–Polanyi constant of step 8, to change, we obtain the observed variations between experimental data and simulation results. As expected, the prediction is more accurate for catalysts in this series whose steaming treatment is closer to that of the relatively mildly steamed catalyst of Ref. (4) from which we have extracted the kinetic parameters for the current analysis. With only one adjustable parameter used to fit all our data, the overall agreement with experimental data is gratifying, and the trends obtained between ΔH_+ and kinetic results are meaningful.

DISCUSSION

The Importance of Carbenium Ion Complex Stabilization

Since the early work of Beaumont and Barthomeuf (33, 34), it has been suggested that all Brønsted acid sites in a dealuminated Y zeolite are of equal acid strength (35–37) and that non-framework Al species may modify these Brønsted sites (8, 9, 38). Although our kinetic model and microcalorimetric results do not allow us to directly probe the effect, if any, of non-framework Al on the catalytic results, our results suggest that the strength of Brønsted acid sites on USY dealuminated via steaming is not constant but depends on steaming severity.

In our earlier analyses of isobutane and 2-methylhexane cracking over Y zeolite-based catalysts (1–4), we used the enthalpy of stabilization on the surface of a carbenium ion relative to a proton to represent the acid strength of a catalyst. Higher values of ΔH_+ indicate decreased stability of a surface carbenium ion relative to a surface proton, which we attribute to a reduction of the Brønsted acid strength of a catalyst. In this more comprehensive study with six catalysts, we found that increasing steaming severity increased ΔH_+ (Fig. 7). This model prediction is consistent with our microcalorimetric data (Figs. 5 and 6), and with the experimental site time yields which decrease substantially with steaming severity (Figs. 8, 9a, and 9b). The important result is the trend of catalyst acid strength with steaming identified by the model and the catalytic ramifications rather than the absolute values of ΔH_+.

Table 2 shows that the kinetic model describes the essential experimental trends over a wide range of steaming treatments by adjusting only the parameter that represents catalyst acid strength, ΔH_+. No other important changes in surface chemistry are necessary.

The decrease in catalyst acid strength with steaming severity appears to increase the activation energy of initiation reactions. This result agrees with expected behavior

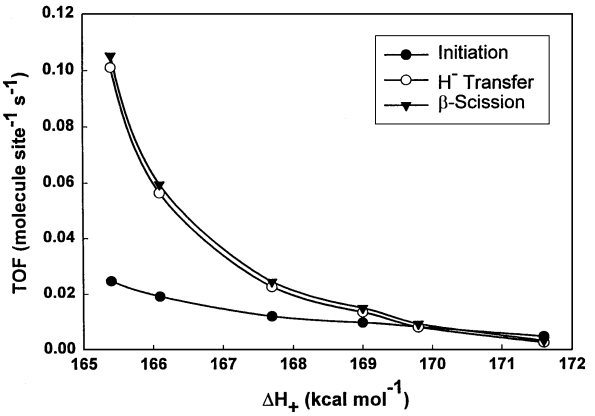

FIG. 10. Turnover frequencies at reactor exit for initiation, hydride ion transfer, and β-scission reactions at 773 K and 15% 2-methylhexane conversion versus ΔH_+.

if, as suggested (39, 40), initiation reactions involve the attack of a proton on a C–C or C–H bond of a hydrocarbon. Figure 10 shows turnover frequencies of initiation, hydride ion transfer, and β-scission reactions at the reactor exit for all six catalysts. As ΔH_+ increases, rates of all surface processes decrease, resulting in the observed reduction in overall activity (Fig. 8). From USY-1 to USY-6, rates of initiation, hydride ion transfer, and β-scission processes decrease by factors of 5, 40, and 33 respectively. Clearly, the rates of hydride ion transfer and β-scission reactions are reduced substantially with increased steaming severity.

If we use the definition of ΔH_+ based on carbenium ion intermediates, then the decrease in rates of hydride ion transfer and β-scission reactions would be related to the decrease in surface coverage of carbenium ions involved in these reactions. Carbenium ion coverage affects rates of all processes with the exception of initiation reactions that are not a strong function of carbenium ion coverage. Thus, a change in ΔH_+ indirectly influences rates of hydride ion transfer and β-scission reactions even though their activation energies are not affected. As ΔH_+ increases, the enthalpy of the equilibrated desorption processes decreases, consequently surface carbenium ion coverage decreases on the weaker Brønsted acid sites while gas phase olefin concentration increases. Our analyses are in agreement with the proposal of Hall and co-workers (41, 42) who first suggested that olefin adsorption–desorption equilibrium controlled carbenium ion concentration or lifetimes on the surface; they also noted that this equilibrium was influenced by Brønsted acid site strength.

In view of recent experimental (27) and theoretical studies (28, 29), it is probably more accurate to use the definition of ΔH_+ based on carbenium ion transition states. In this case, the decrease in rates of hydride ion transfer and β-scission reactions caused by increased steaming severity is related to the decrease in reactivity of surface alkoxy species. These species are first formed from the alkane reactant by initiation reactions, the rates of which decrease with severity of steam treatment. Further decrease in rates of hydride ion transfer and β-scission reactions with steaming is caused by an increase in activation energies and a decrease in rate constants for these reactions, while equilibrium constants for desorption processes leading to olefin formation remain unchanged.

Our analysis is simplified by the fact that we are comparing catalysts within the same family and the relevance of ΔH_+ may be readily described in terms of Brønsted acidity. In other cases such analyses may be quite complex; the work of Parrillo *et al.* (43) is a case in point. They found that H-[Al]ZSM-5, H-[Ga]ZSM-5, and H-[Fe]ZSM-5 all contained Brønsted acid sites of the same strength as measured by ammonia and pyridine microcalorimetry. However, whereas the Ga and Al isomorphs were active for hexane cracking and propene oligomerization, H-[Fe]ZSM-5 was inactive. Furthermore propene did not chemisorb irreversibly at room temperature on H-[Fe]ZSM-5 even though isopropylamine cations were readily formed and decomposed on the catalyst. The fact that the catalyst is inactive implies that the value of ΔH_+ must be relatively high. This high value would lead to low rates of initiation reactions involving the hexane reactant and even lower rates of hydride ion transfer and β-scission propagation reactions.

In other examples, Lombardo *et al.* (41, 42) have shown mordenite to be extremely active for cracking isobutane and neopentane with a high propensity for hydride ion transfer and paraffinic products. This behavior again translates into the ability of the catalyst to have a low value of ΔH_+ indicating strong acidity and high surface coverage of carbenium ion intermediates or transition states. Eder and Lercher (44) note that heats of adsorption of hydrocarbons depend on the size of the molecular sieve cavity; this effect could influence the stability of surface intermediates or transition states, leading to different coverages for different molecular sieves.

We reiterate that in its simplest form ΔH_+ represents the strength of Brønsted acid sites, but more generally it represents the stabilization of a carbenium ion complex (intermediate or transition state) on a reactive site. Such stability on different systems may be influenced by surface properties other than only acidity. The key to surface carbenium ion chemistry is surface carbenium ion coverage, whether as an intermediate or a transition complex. Therefore, the enthalpy of stabilization of carbenium ion complexes as reflected in the parameter ΔH_+ plays an important role in determining reactivity.

Catalytic Cycles

Earlier (4, 5), we showed how 2-methylhexane cracking could be described by various catalytic cycles (see Fig. 11). Three catalytic cycles are dominant. Initiation/desorption

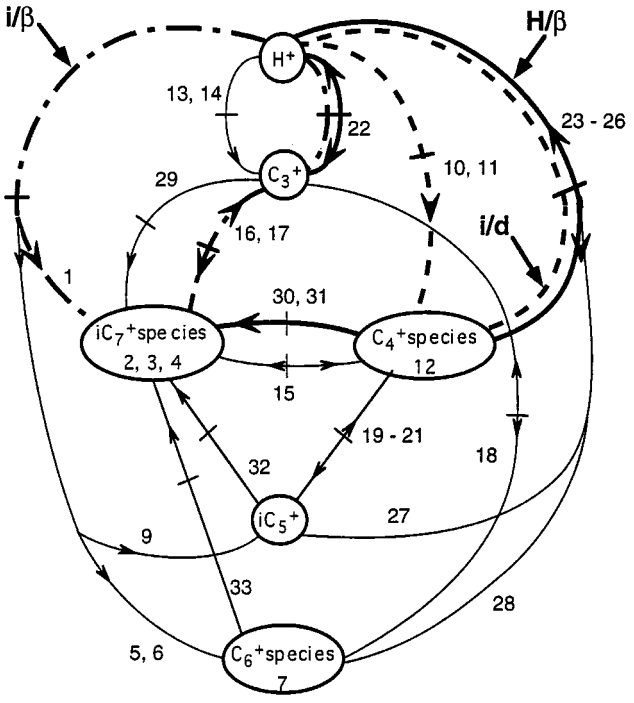

FIG. 11. Catalytic cycles for 2-methylhexane cracking over USY zeolite-based catalysts at 773 K and 15% conversion at the reactor exit as composed of steps 1–33 in Fig. 1. Examples of initiation/β-scission (i/β), initiation/desorption (i/d), and hydride ion transfer/β-scission (H/β) cycles are shown.

cycles form paraffins by initiation and olefins by desorption of the resulting carbenium ion. These cycles produce paraffins and olefins with three or more carbon atoms at a ratio of 1 : 1. Initiation/β-scission cycles form large carbenium ions with six or seven carbon atoms that undergo β-scission to give C_3 and C_4 olefins. Hydride ion transfer/β-scission cycles include hydride ion transfer reactions followed by β-scission reactions that produce C_3 and C_4 paraffins and olefins at a 1 : 1 ratio. Thus, the product of the reaction consists mainly of these paraffins and olefins at a ratio close to or lower than 1 with only minor amounts of other products. Figure 12 clearly demonstrates that increasing the severity of steaming has little effect on the overall chemistry; selectivities of C_3, C_4, and $C_5 + C_6$ hydrocarbons are independent of steaming severity and ΔH_+. These selectivities are also independent of conversion (4). These results indicate that no new reactions need to be invoked to describe catalytic cracking. However, steaming affects rates of individual reactions and thus influences the contribution of each cycle; the rates of these cycles determine overall activity and selectivity.

Initiation and hydride ion transfer cycles are the two cycles where 2-methylhexane is consumed, and therefore these processes determine catalytic activity. Since rates of initiation processes do not decrease with steaming severity as much as rates of hydride ion transfer processes (Fig. 10),

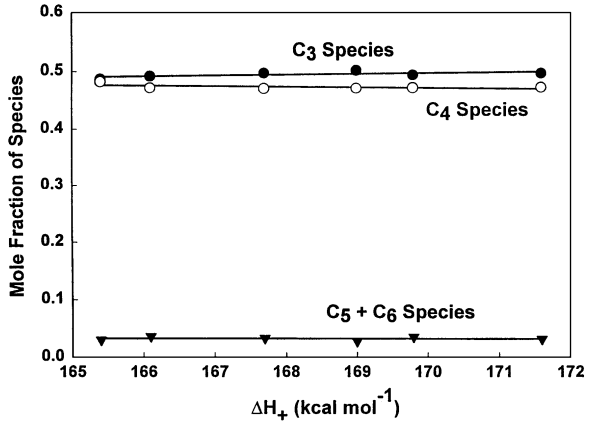

FIG. 12. Simulated and experimental distributions in the gas phase of C_3, C_4, and $C_5 + C_6$ species at 773 K and 15% 2-methylhexane conversion versus ΔH_+. Points represent experimental data.

their relative contribution to the catalytic activity increases with steaming more than three times (Fig. 13). Initiation and hydride ion transfer cycles are also the main pathways through which olefins are produced. As steaming severity increases, the model predicts that the relative importance of initiation processes for olefin formation increases whereas the contribution of β-scission reactions decreases. The decrease in the contribution of β-scission reactions to olefin formation shown in Fig. 13 is caused by the decrease in the importance of the hydride transfer/β-scission cycles relative to the initiation cycles. As shown in Fig. 14, the relative rate of the initiation/β-scission cycles increases by a factor of 3.9 as steaming severity increases. This increase in the relative rates of the initiation/β-scission cycles results in an increase in olefin selectivity, since these cycles produce two olefins with three or more carbon atoms for every 2-methylehaxane molecule converted. The relative rates of the initiation/desorption cycles also increase by a

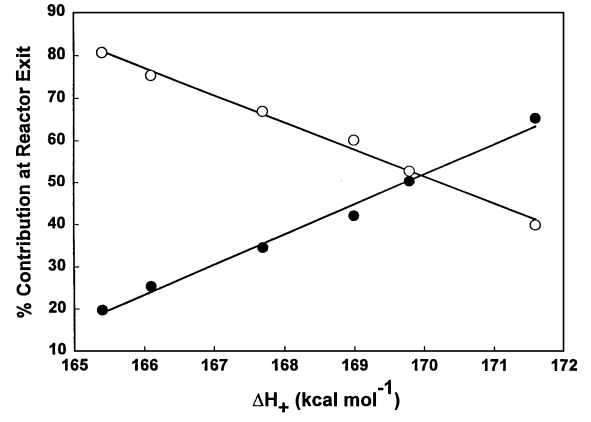

FIG. 13. Percentage contribution at the reactor exit of total olefin formation (TOF) of initiation reactions to catalytic activity (closed circles) and β-scission cycles to the TOF of the total olefin formation (open circles) at 773 K and 15% 2-methylhexane conversion versus ΔH_+.

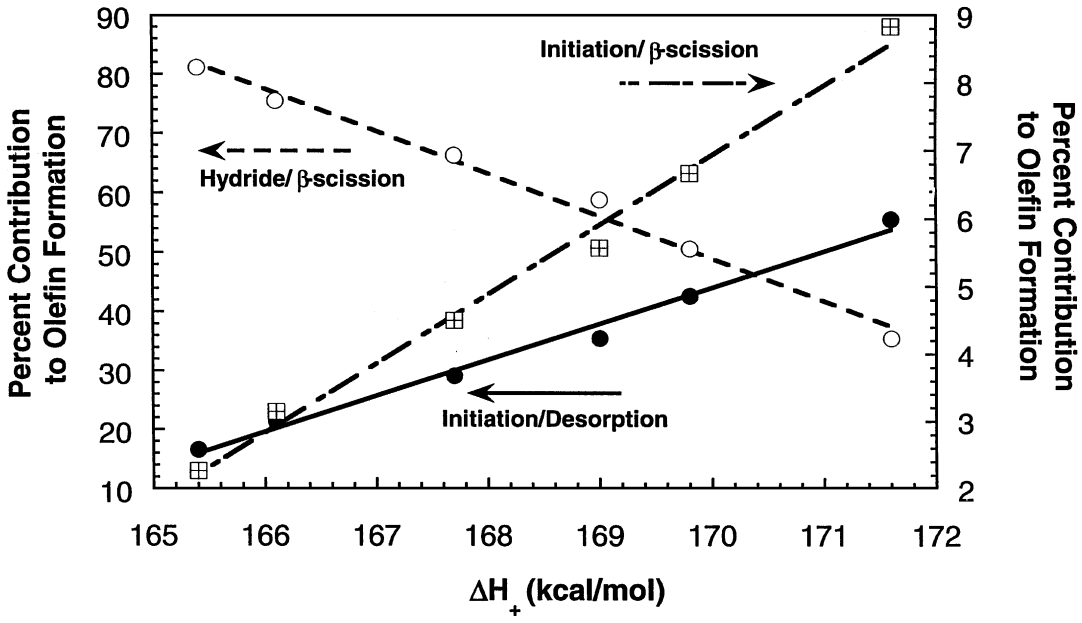

FIG. 14. Relative contribution to the TOF of olefin formation by the initiation/β-scission (two net olefins with three or more carbon atoms per TOF), initiation/desorption (one net olefin with three or more carbon atoms per TOF), and hydride transfer/β-scission cycles (one net olefin with three or more carbon atoms per TOF). Data shown are model estimates at the reactor exit.

factor of 3.3. However, this change does not affect the paraffin to olefin selectivity, because these cycles make paraffins and olefins with three or more carbon atoms at a ratio of 1 : 1, which is the same as the hydride ion transfer/β-scission cycles.

CONCLUSIONS

An important factor in solid acid catalysis is the stability of surface carbenium ion complexes as reflected in the parameter ΔH_+. This parameter may be defined as (a) the heat of formation of a surface *carbenium ion intermediate* by reaction of a gaseous olefin with a Brønsted acid site relative to the heat of formation of a gaseous carbenium ion by reaction of an olefin with a gaseous proton or (b) the enthalpy of a *carbenium ion transition state* relative to the enthalpy of stabilization of a surface proton. The latter definition is more in line with recent experimental (27) and theoretical (28, 29) studies. Both cases are kinetically equivalent leading to the same conclusions. And in both cases, ΔH_+ is determined by Brønsted acid strength.

By using steam treatment, the simplest but commercially important way to modify a Y-based FCC catalyst, we altered the number and strength of Brønsted acid sites. To simulate the experimental results on six samples steamed under different conditions, the model predicted that the value of ΔH_+ increased with increased steaming severity. Higher values of ΔH_+ indicate increased difficulty of weaker Brønsted acid sites to stabilize carbenium ion intermediates or transition states on a site relative to a proton. Therefore, activity per Brønsted acid site decreases as steaming severity increases and the acid strength of sites decreases.

The model predicts changes in rates of hydride ion transfer without the need for two adsorbed hydrocarbon species on catalytic sites in close proximity (14, 45, 46). Our model, where a surface carbenium ion reacts with a gas phase or physisorbed molecule, adequately simulates the essential effects of steaming on the rates of these processes. Rates of bimolecular processes decrease with steaming not because the number of acid sites in close proximity is reduced, but because the activation energy increases or the concentration of carbenium ions on the catalytic surface decreases as the strength of Brønsted acid sites decreases.

Increased steaming severity does not change surface chemistry and the catalytic cycles that describe the overall reaction. The model is able to accurately predict essential experimental trends over all catalysts by adjusting only the parameter that reflects catalyst acid strength. However, as acid strength decreases the relative rates of various cycles change. Rates of cycles that produce paraffins are affected more than those that produce olefins. Steaming does not affect initiation/β-scission cycles to the same extent as it affects initiation/desorption and hydride ion transfer/β-scission cycles. Therefore, olefin selectivity increases as steaming severity increases.

ACKNOWLEDGMENTS

We thank to Marty Gonzalez and Kevin Fogash for carrying out the microcalorimetry measurements, Gale Hodge for the FTIR work, and Randy

Cortright for valuable discussions. We also sincerely appreciate the work done by the late Stan Koziol who carried out all the kinetic measurements. This work was partially supported by funds provided by Engelhard Corporation and the Office of Basic Energy Sciences of the U.S. Department of Energy (DE-FG02-84ER13183). This work was also supported in part by the U.S. Environmental Protection Agency and the Center for Clean Industrial and Treatment Technologies

REFERENCES

1. Yaluris, G., Rekoske, J. E., Aparicio, L. M., Madon, R. J., and Dumesic, J. A., *J. Catal.* **153**, 54 (1995).
2. Yaluris, G., Rekoske, J. E., Aparicio, L. M., Madon, R. J., and Dumesic, J. A., *J. Catal.* **153**, 65 (1995).
3. Yaluris, G., Madon, R. J., Rudd, D. F., and Dumesic, J. A., *Ind. Eng. Chem. Res.* **33**(12), 2913 (1994).
4. Yaluris, G., Madon, R. J., and Dumesic, J. A., *J. Catal.* **165**, 205 (1997).
5. Cortright, R., Dumesic, J. A., and Madon, R. J., *Top. Catal.* **4**, 15 (1997).
6. Engelhardt, G., Lohse, U., Patzelova, V., Magi, M., and Lippmaa, E., *Zeolites* **3**, 233 (1983).
7. Gelin, P., and Des Courieres, T., *Appl. Catal.* **72**, 179 (1991).
8. Fritz, P. O., and Lunsford, J. H., *J. Catal.* **118**, 85 (1989).
9. Beyerlein, R. A., McVicker, G. B., Yacullo, L. N., and Ziemiak, J. J., *J. Phys. Chem.* **92**, 1967 (1988).
10. Kuehne, M. A., Babitz, S. M., Kung, H. H., and Miller, J. T., *Appl. Catal. A* **166**, 293 (1998).
11. Shertukde, P. V., Hall, W. K., Dereppe, J.-M., and Marcelin, G., *J. Catal.* **139**, 468 (1993).
12. Bamwenda, G. R., Zhao, Y. X., Groten, W. A., and Wojciechowski, B. W., *J. Catal.* **157**, 209 (1995).
13. Wang, Q. L., Giannetto, G., and Guisnet, M., *J. Catal.* **130**, 471 (1991).
14. Pine, L. A., Maher, P. J., and Wachter, W. A., *J. Catal.* **85**, 466 (1984).
15. Corma, A., Faraldos, M., Martínez, A., and Mifsud, A., *J. Catal.* **122**, 230 (1990).
16. Corma, A., Faraldos, M., and Mifsud, A., *Appl. Catal.* **47**, 125 (1989).
17. Madon, R. J., *J. Catal.* **129**, 275 (1991).
18. Chen, D., Sharma, S., Cardona-Martínez, N., Dumesic, J. A., Bell, V. A., Hodge, G. D., and Madon, R. J., *J. Catal.* **136**, 392 (1992).
19. Haden, W. L., and Dzierzanowski, F. J., U.S. Patents 3,506,594 (1970) and 3,647,718 (1972).
20. Brown, S. M., Durante, V. A., Reagen, W. J., and Speronello, B. K., U.S. Patent 4,493,902 (1985).
21. Madon, R. J., Koermer, G. S., and Macaoay, J. M., U.S. Patent 5,395,809 (1995).
22. Sohn, J. R., DeCanio, S. J., Lunsford, J. H., and O'Donell, D. J., *Zeolites* **6**, 225 (1986).
23. Handy, B. E., Sharma, S. B., Spiewak, B. E., and Dumesic, J. A., *Meas. Sci. Technol.* **4**, 1350 (1993).
24. Yaluris, G., "Factors Controlling the Activity and Selectivity of Hydrocarbon Reactions on Acidic Catalysts," Ph.D. thesis. Univ. of Wisconsin, Madison, 1995.
25. Dumesic, J. A., Rudd, D. F., Aparicio, L. M., Rekoske, J. E., and Treviño, A. A., "The Microkinetics of Heterogeneous Catalysis." Am. Chem. Soc., Washington, D.C., 1993.
26. Leftin, H. P., and Hall, W. K., "Actes Deuxieme Int. Congr. Catal.," Vol. 1, p. 1353. Technical publ., 1960; Lombardo, E. A., Dereppe, J. M., Marcelin, G., and Hall, W. K., *J. Catal.* **114**, 167 (1988); Zardkoohi, M., Haw, J. F., and Lunsford, J. H., *J. Am. Chem. Soc.* **109**, 5278 (1987).
27. Aronson, M. T., Gorte, R. J., and Farneth, W. E., *J. Catal.* **98**, 434 (1986); **105**, 455 (1987); Aronson, M. T., Gorte, R. J., White, D., and Farneth, W. E., *J. Am. Chem. Soc.* **111**, 840 (1989); Kazansky, V. B., *Acc. Chem. Res.* **24**, 379 (1991); Haw, J. F., Richardson, B. R., Oshiro, I. S., Lazo, N. D., and Speed, J. A., *J. Am. Chem. Soc.* **111**, 2052 (1989); Farneth, W. E., and Gorte, R. J., *Chem. Rev.* **95**, 615 (1995).
28. Malkin, V. G., Chesnokov, V. V., Paukshtis, E. A., and Zhidomirov, G. M., *J. Am. Chem. Soc.* **112**, 666 (1990); Rigby, A. M., Kramer, G. J., and van Santen, R. A., *J. Catal.* **170**, 1 (1997); Natal-Santiago, M. A., de Pablo, J. J., and Dumesic, J. A., *Catal. Lett.* **47**, 119 (1997); Kazansky, V. B., and Sechenya, I. N., *J. Catal.* **119**, 108 (1989); Kazansky, V. B., Frash, M. V., and van Santen, R. A., *Catal. Lett.* **28**, 211 (1994); **48**, 61 (1997); Blaszkowski, S. R., and van Santen, R. A., *Top. Catal.* **4**, 145 (1997).
29. Natal-Santiago, M. A., Alcala, R., and Dumesic, J. A., *J. Catal.* **181**, 124 (1999).
30. Biaglow, A. I., Gittleman, C., Gorte, R. J., and Madon, R. J., *J. Catal.* **129**, 88 (1991).
31. Biaglow, A. I., Parrillo, D. J., and Gorte, R. J., *J. Catal.* **144**, 193 (1993).
32. Biaglow, A. I., Parrillo, D. J., Kokotailo, G. T., and Gorte, R. J., *J. Catal.* **148**, 213 (1994).
33. Beaumont, R., and Barthomeuf, D., *J. Catal.* **26**, 218 (1972).
34. Beaumont, R., and Barthomeuf, D., *J. Catal.* **27**, 45 (1972).
35. Barthomeuf, D., *Mater. Chem. Phys.* **17**, 49 (1987).
36. Mikovsky, R. J., and Marshall, J. F., *J. Catal.* **44**, 170 (1976).
37. Dempsey, E., *J. Catal.* **33**, 497 (1974); **39**, 155 (1975).
38. Mirodatos, C., and Barthomeuf, D., *J. Catal.* **114**, 121 (1988).
39. Haag, W. O., and Dessau, R. M., *in* "Proceedings, 8th International Congress on Catalysis, Berlin, 1984," Vol. 2, p. 305. Dechema, Frankfurt-am-Main, 1984.
40. Corma, A., Planelles, J., Sánchez-Marín, J., and Tomás, F., *J. Catal.* **93**, 30 (1985).
41. Lombardo, E. A., and Hall, W. K., *J. Catal.* **112**, 565 (1988).
42. Lombardo, E. A., Pierantozzi, R., and Hall, W. K., *J. Catal.* **110**, 171 (1988).
43. Parrillo, D. J., Lee, C., Gorte, R. J., White, D., and Farneth, W. E., *J. Phys. Chem.* **99**, 8745 (1995).
44. Eder, F., and Lercher, J. A., *J. Phys. Chem.* **101**, 1273 (1997).
45. Wielers, A. F. H., Vaarkamp, M., and Post, M. F. M., *J. Catal.* **127**, 51 (1991).
46. Giannetto, G., Sansare, S., and Guisnet, M., *J. Chem. Soc. Chem. Commun.* 1302 (1986).